

Analysis of seismic wave propagation in geothermal reservoirs

Flavio Poletto, Biancamaria Farina, José M. Carcione and Giorgia Pinna

OGS – Istituto Nazionale di Oceanografia e di Geofisica Sperimentale,
Borgo Grotta Gigante 42/c 34010 Sgonico (Trieste), Italy
fpoletto@inogs.it

Keywords: Seismic waves, temperature, pressure, geothermal reservoirs.

ABSTRACT

We present a review summary of the theory of seismic wave propagation in geothermal reservoir, including temperature and pressure effects based on the Arrhenius equation and poro-viscoelasticity. We quantify the effects of the melting rate point on the seismic velocities, and consider surface and borehole acquisition geometries. We perform wavefield simulations for geothermal areas located at different depths in dissimilar geological contexts.

1. INTRODUCTION

In recent years, rheological studies have been focused to incorporate temperature and melting in the study of seismic wave properties (Jaya et al. 2010) and develop a theory of wave propagation in hot and very-hot geothermal regions with partial melting or melting conditions, such as the brittle-ductile transition (BDT) (Carcione and Poletto, 2013). These approaches have been subsequently used to enable the utilization of seismic methods by developing full-waveform viscoelastic simulation codes for arbitrary geothermal environments (Carcione et al., 2014), including temperature effects through the Arrhenius equation, and confining and pore pressure, with fluids at different phase states (Carcione et al., 2017). The methodology provides synthetic seismograms for geothermal regions, that can be used for a sensitivity analysis of the seismic properties at different rheological conditions (Poletto, et al. 2018), and the study of conductive and convective geothermal systems (Farina et al., 2019).

A preliminary analysis was applied to models obtained from the literature, including geothermal scenarios in Mexico, investigated in the framework of the GEMex H2020 project. This involves a calibrated choice of the rheological, structural and geothermal parameters at the subsurface conditions (Farina et al., 2016). This task required an estimation of the characteristic properties with suitable approximations for the given geological conditions.

Here, we present a review summary of the theory and numerical simulation of seismic wave propagation focused on surface and borehole geometries, and a

discussion of the physical modelling conditions for geothermal areas located at different depths and at different geological contexts. We present examples of wave-field simulation and analysis of the related physical and seismic parameters, and discuss their impact for the calculation of the results.

2. THEORY

2.1 Burgers-Arrhenius model

According to experimental studies, linear viscoelastic models can be used to describe the behaviour of ductile media. Carcione and Poletto (2013) studied the seismic properties of rocks with a ductile behaviour on the basis of variations of the shear modulus as a function of temperature. They proposed a rheology based on the Burgers mechanical model, which is obtained by adding a dashpot (Burgers viscosity), responsible for the steady-state viscous flow, to the Zener model.

The Zener model is used to describe viscoelastic deformation without viscous flow, obtained as the limit of infinite Burgers viscosity. Carcione and Poletto (2013) modelled the effects of anisotropy, seismic attenuation and steady-state creep flow. The frequency-domain Burgers shear modulus is expressed as a function of the seismic relaxation times (τ_σ and τ_ε) of the unrelaxed shear modulus μ_0 , and of the flow viscosity η that describes the ductile behaviour related to the shear deformation:

$$\mu_B(\omega) = \frac{\mu_0(1 + i\omega\tau_\varepsilon)}{1 + i\omega\tau_\sigma - \frac{i\mu_0}{\omega\eta}(1 + i\omega\tau_\varepsilon)}, \quad [1]$$

where ω is the angular frequency and $i = \sqrt{-1}$.

The high temperature effects on seismic wave losses are related to the Burgers viscosity and are solely due to shear deformations. Carcione and Poletto (2013) introduced the viscosity η related to the steady-state creep rate $\dot{\varepsilon}$, which is in turn related to the temperature T through the Arrhenius equation:

$$\eta = \frac{\tau_0}{2\dot{\varepsilon}} = \frac{1}{2A_\infty} \tau_0^{1-n} \exp(E/RT), \quad [2]$$

where τ_0 is the octahedral stress used to describe deformation of the ductile medium. The octahedral stress (see Carcione and Poletto, 2013) is a function of

the stress components along the principal axes and takes into account the additional effects due to the anisotropic tectonic stress related to tectonic activity. A_∞ and n are Arrhenius constants, and E is the activation energy of the medium. $R=8.3144$ J/mol/K is the gas constant and T is the absolute temperature. The complex frequency-dependent compressional (P) and shear (S) phase-velocities are

$$V_P = \sqrt{\frac{K + 4\mu_B(\omega)/3}{\rho}} \quad \text{and} \quad V_S = \sqrt{\frac{\mu_B(\omega)}{\rho}}, \quad [3]$$

where K and ρ are the rock modulus and density, respectively.

2.2 Gassman-Burgers model

To simulate full-waveform seismic propagation in poro-viscoelastic geothermal reservoirs including temperature, Carcione et al. (2014) implemented an algorithm based on the Burgers mechanical model, which includes the transient creep of the Zener model and the steady-state creep of the Maxwell model. They simulated seismic wave propagation in heterogeneous anelastic media in the presence of the brittle-ductile transition (BDT), where memory variables were implemented to solve the differential equations in the time domain. The equations are developed in the velocity-stress formulation by using eight memory variables for 2D P-S wave propagation.

Carcione et al. (2017) extended the theory to poro-viscoelastic media. They explicitly modelled the effects of saturating fluids, using water and steam at various pressure-temperature conditions, considering supercritical states. The approach yields the wet-rock Gassmann-Burgers bulk and shear moduli

$$K_G = K_m + \alpha^2 M \quad \text{with} \quad \alpha = 1 - \frac{K_m}{K_s}, \quad [4]$$

and

$$M = \frac{K_s}{1 - \phi - K_m/K_s + \phi K_s/K_f}, \quad [5]$$

where K_m , K_s and K_f are the dry-rock, mineral and fluid bulk moduli, respectively, and ϕ is the porosity .

2.3 Seismic velocity

The properties in poro-viscoelastic media are characterized by seismic velocity and attenuation Q^{-1} , where Q is the quality factor. Here, we pay attention to the velocity.

The complex phase velocities are obtained on the basis of equations (3) (Carcione and Poletto, 2013), by substituting the rock-frame bulk modulus K with the wet-rock bulk modulus K_G and the rock density ρ with the bulk density $\rho_b = (1 - \phi)\rho + \phi\rho_f$, where ρ_f is

the fluid density. Important and characteristic velocity variations are calculated for melting conditions and the presence of the BDT.

3. MELTING CONDITIONS

To illustrate typical seismic properties in reservoirs as a function of temperature, we present a preliminary overview of the rock's melting behaviour in relation to the thermodynamic conditions, which are expressed in our analysis by the Arrhenius parameters (eq. [2]). For this purpose, we assume a medium with uniform properties, neglecting the presence of fluids and pore pressure as an approximation. In these examples we refer to the amphibolite rock sample of Popp and Kern (1994), as representative of the properties of a crustal rock, including intrinsic attenuation Q_0 (Table 1).

We use the confining pressure at variable depth z to calculate the octahedral stress (Carcione and Poletto, 2013). Then, keeping constant the other properties, we vary the Arrhenius stress parameter-exponent n , the amplitude A (for convenience here we use the simplified notation A for A_∞), and the rock sample activation energy E .

This provides us a set of characteristic curves representing the behaviour of the partially or completely melted rock versus depth and temperature. This analysis, based on literature laboratory rheological data, is mainly aimed at describing and better understanding the seismic properties in the presence of shear viscosity by creep flow, a function of the Arrhenius parameters. A similar analysis can be extended to rocks of other types, such as those of volcanic environments.

Table 1: Rock parameters used for the calculation of the melting conditions.

Property	Value	Unit
ρ	3000	Kg/m ³
K_0	67.1	GPa
K_S	89.4	GPa
μ_0	41.4	GPa
Q_0 (at 10 Hz)	122	

To perform the analysis, we consider a range of three values for each quantity: the depth z (m), the stress exponent n , the amplitude A (MPa ^{n} s ^{-1}), and the activation energy E (kJ mol ^{-1}). For convenience, we describe the configurations using the index values 1, 2, 3 for each of them as described in Table 2. For the activation energy, this table shows the energy factor E_F used in the calculation of $E = E_F \times E_0$, where $E_0 = 134$ (kJ mol ^{-1}) is a reference value (Carcione and Poletto, 2013). For example the ordered index values 1, 3, 2, 1 mean that we have used the values z_1 , n_3 , A_2 and E_1 .

Table 2: Index table.

Index:	1	2	3
z (km)	5	10	20
n	1	2	4
A (MPa $^{-n}$ s $^{-1}$)	10^{-6}	10^{-2}	10^{10}
E_F	0.5	1	2

Figure 1 shows the effect of the activation energy by E_F on the shear velocity (V_S) versus temperature, while the other quantities are maintained constant as denoted by the indexes 3, 2, 2, $j=(1,\dots,3)$. The melting effect in the velocity is clear. This example shows the intuitive result that a lower temperature is required to melt with a lower activation energy. Similar curves are obtained for compressional P-waves, with the difference that for S waves the velocity after melting is zero (a liquid), while for P-waves the velocity is greater than zero.

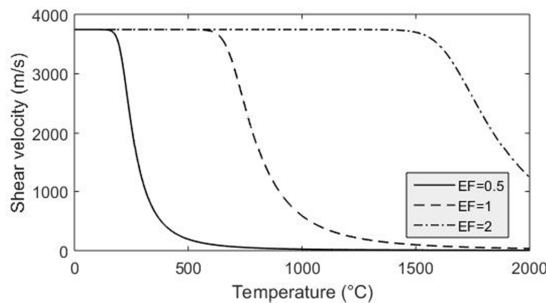
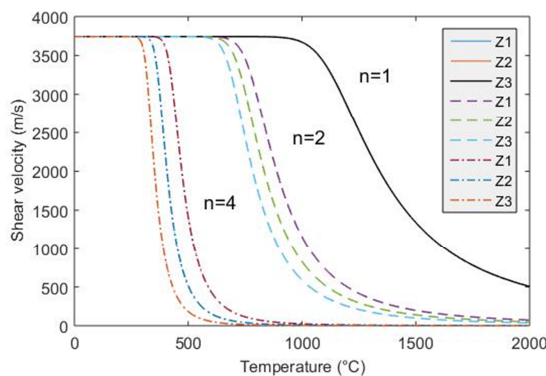
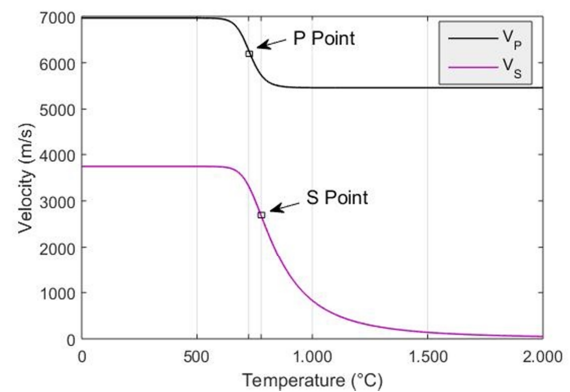
**Figure 1:** Shear velocity curves showing the melting effects of temperature with different activation energies. Case 3, 2, 2, $j=(1,\dots,3)$.

Figure 2 shows the behaviour of the S-wave velocity for different depths z and stress index n . The index values of A and E are set 2 and 2, respectively. The exponent index n governs the effects of confining pressure through the octahedral stress, and $n = 1$ means that there is no dependence on confining pressure, hence on depth. For this reason, all the curves with $n = 1$ are superimposed. For $n > 1$, the melting effects occur at lower temperatures for higher depths, hence at higher confining pressures.

**Figure 2:** Shear velocity curves showing the melting effects of temperature with different depths and exponent index n .

These results pose the problem to estimate the depth of melting under different conditions. We introduce two criteria based on seismic velocity as a function of temperature. Similar considerations can be made also for attenuation (e.g., Poletto et al., 2018), which is significantly affected because the Burgers viscosity decreases due to the thermally induced creep flow. However, it is in general more difficult to measure the Q factor than the seismic velocity. For this reason, we introduce two criteria to characterize the melting conditions, based on the behaviour of P- and S-waves. The P-wave and S-wave velocity curves are different not only in magnitude, but also because the P-wave velocity decreases from the velocity of a solid to that of a liquid (full melting). Conversely, the shear velocity in the melted rock fluid at high temperatures is zero. These effects can be observed in Figure 3, where we show the temperature-velocity profiles of the case identified by indexes 2, 2, 2, 2.

**Figure 3:** Characteristic melting-rate points for P and S waves at different temperatures (case 2, 2, 2, 2).

We see that the curve of the P wave has a sort of ‘symmetry’ around its flexing point, while the curve of the S wave is ‘asymmetric’ with a trend tending to zero for high temperatures. We keep as characteristic temperature point the inflexion point, i.e., the point where the derivative, i.e., the negative melting rate, is minimum (absolute maximum)

$$\frac{\partial V_{P,S}}{\partial T} = \min, \quad [6]$$

after an initial decrease and then an increase with increasing temperature. These points are indicated by arrows (Fig. 3), and correspond to 724 °C and 778 °C for P and S waves, respectively. We define these points where the melting effect has its maximum rate (negative rate for velocity) as the characteristic melting-rate points. In other words, we observe the ‘central’ melting point in the velocity curve, rather than an ‘initial’ one.

Figure 4 shows the temperature-depth curves of the melting-rate points for the P and S waves (case $z, n, 2, 2$) calculated with different values of the n Arrhenius stress exponent. Using an exponent $n > 1$, we obtain a decrease of the melting temperature with increasing

depth. In this example, the maximum confining pressure is 0.589 GPa at 20 km and the pressure increases by 0.0294 GPa/km.

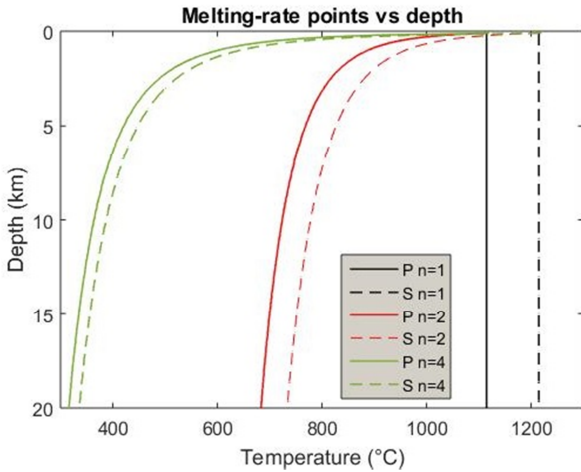


Figure 4: Characteristic melting-rate points of the P and S waves versus temperature and depth (case z, n, 2, 2).

In Figure 5, we compare the characteristic melting-rate curve calculated for P waves (case z, 2, 2, 2) with temperature curves obtained by different linear temperature gradients: TG = 10 °C/km and TG = 5 °C/km. This figure gives an estimate of the melting depth for an assumed temperature profile, accordingly with our definition of melting-rate points (marked by small rectangles in the plot) defined as the inflexion point (maximum negative rate for the velocity) in the temperature-velocity profile.

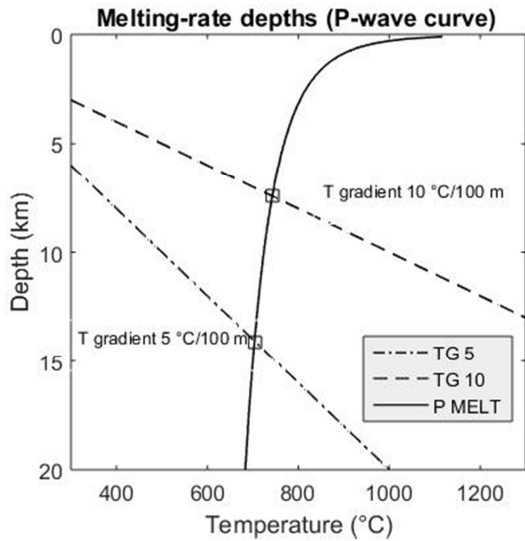


Figure 5: Estimation of melting points at depth according to the velocity-inflexion point definition (case z, 2, 2, 2).

The results in Figures 4 and 5 have trends versus depth similar to and consistent with those of the melting temperature-pressure curves obtained for crustal wet rocks (Schilling et al., 2006; Lambert and Wyllie, 1972), in our case characterized by the rock properties of Table 1.

In the next section, we extend the analysis to compute wavefield simulations with seismic properties in heterogeneous poro-viscoelastic geothermal media, including fluids and pressure.

4. SIMULATIONS

We calculate synthetic full waveforms focusing on the superhot geothermal field of Los Humeros, the largest active caldera located in the northernmost part of the eastern sector of the Trans-Mexican volcanic belt (Carrasco-Núñez et al., 2017). This is one of the two field sites studied by the joint European-Mexican GEMex project (funded from the European Union's Horizon 2020 research and innovation programme under grant agreement No. 727550).

In this context, we consider two geothermal scenarios in which the seismic response is sensitive to the high temperature and pressure conditions.

4.1 Proximity to melting formations

In the first scenario, we consider proximity to a magma chamber with melting formations. We use the geological and temperature model proposed by Verma et al. (1990), located along the profile shown in the map by the red line in Figure 6.

In this model, Verma et al. (1990) proposed the presence of a circular magma chamber under the caldera, with two cylindrical chimneys at the top, that they located according to geochemical and geological studies on some wells near and along the line.

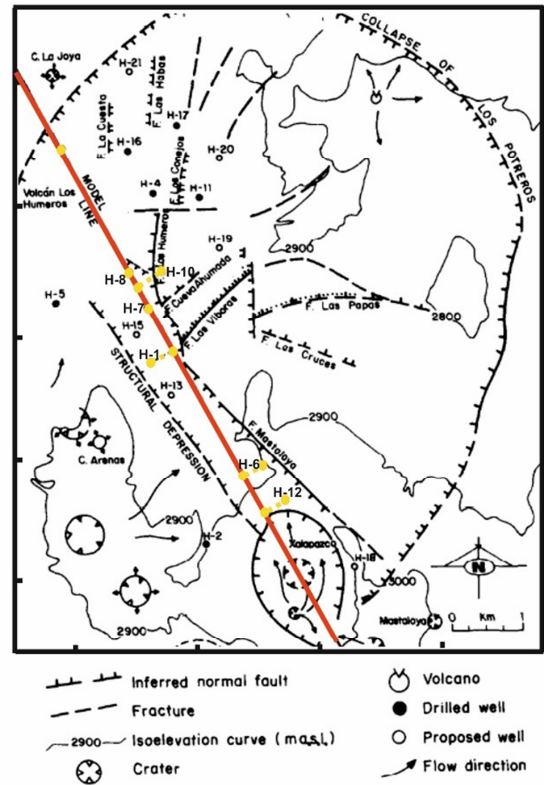


Figure 6: Location of the seismic line (red) with the position of drilled wells (modified after Verma et al., 1990).

A view of the chimney, with the corresponding lithological units of the line proposed by Verma et al. (1990), is shown in Figure 7, with the isotherms superimposed to the lithology section. In the first scenario, we neglect the presence of the hotter chimney, in a medium with temperature calculated assuming a linear gradient between the isotherms.

Assuming these lithological units and isotherms, we construct the geological model. Then we simulate the wave-fields by using the rock-frame and Arrhenius properties given in Table 3. For all the formations we assume $V_p/V_s = 2$, porosity 5 % and pure water as geothermal fluid, as an approximation. We simulate the non-melting and melting condition by changing only the Arrhenius parameters, denoted as A1 and A2, respectively, of the last two layers, and compare the results to analyse the sensitivity of the seismic response to the thermal properties. To evaluate the melting conditions we used the analysis of the case (2, 2, 2, 2) of the previous section. For this purpose, we extend the model to a depth of 9.9 km.

Figure 8 shows the geological model for a VSP synthetic experiment with the seismic source at depth (3.6 km), located at a lateral position with respect to the right chimney, to simulate a natural micro-crack, or passive SWD measurements from a source well (Poletto and Miranda, 2004). The VSP is extended from the surface to 8.5 km depth (Fig. 9), thus entering the zone of melting. Obviously this condition is not realistic because of the high recording depth in melting areas, but for limited hot-zone approaching by ICDP (International Continental Scientific Drilling) wells. For the numerical simulation we use the 2D Burgers-Gassmann full-waveform propagation code in poro-viscoelastic media with temperature of Carcione et al. (2017). The grid pixel size is 30 m × 30 m.

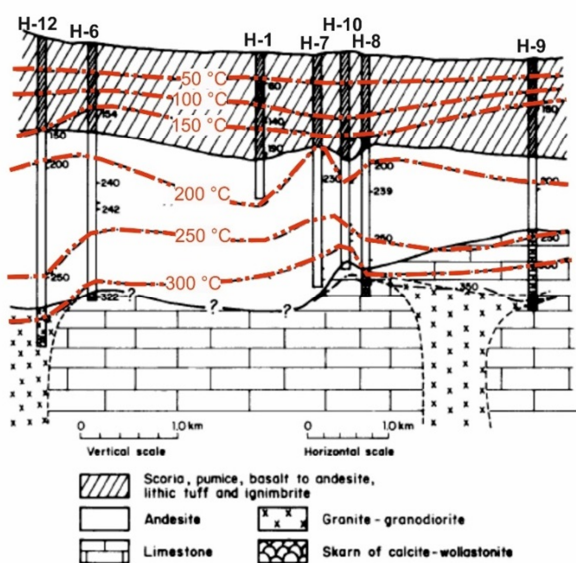


Figure 7: Geological model of the line in Figure 6 with superimposed isotherm (modified after Verma et al., 1990).

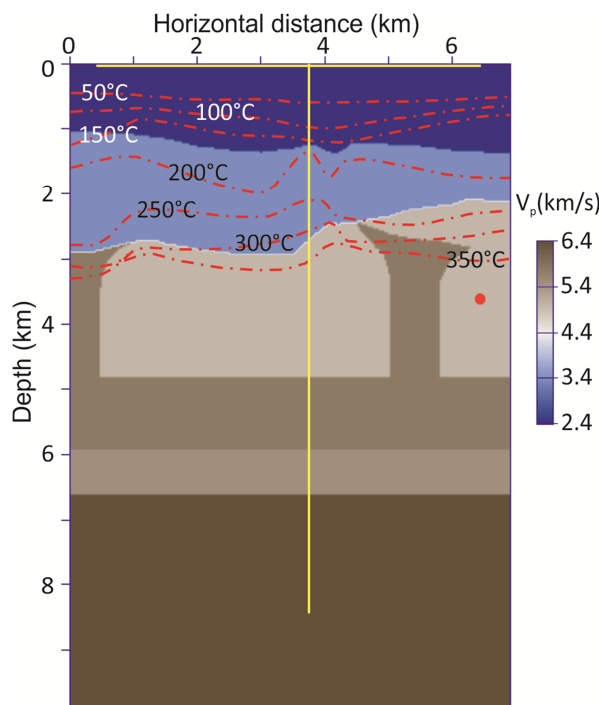


Figure 8: Input P-velocity model of the rock frame used for synthetic simulation. The yellow lines indicate the VSP and the surface profiles, the red star denotes source.

Figure 9 shows the temperature model used for the VSP experiment without and with melting in the presence of different Arrhenius values (A1) and (A2) in Table 3, respectively.

We can observe differences in the prediction signals, namely up-going wave-fields, which can be observed from shallower positions before reaching the melting zone.

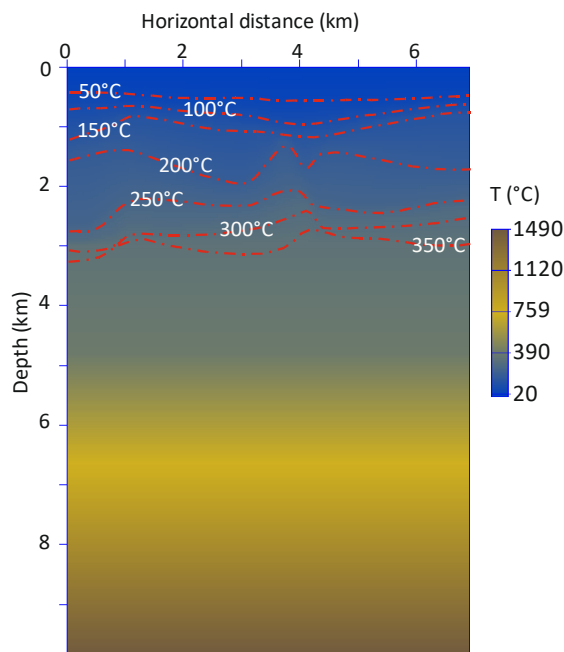


Figure 9: Temperature model used for synthetic simulation of the VSP experiment.

Table 3: Seismic and Arrhenius parameters used for the model of Los Humeros.

Rock Type	V_p (m/s)	ρ (g/cm^3)	References for Arrhenius parameters	A ($\text{MPa}^{-n} \text{s}^{-1}$)	n	E (kJ/mol)
Tuff, Pumice, Basalt, Andesite	2400	2.140	Fernández and Ranalli (1997)	10^{-2}	1.8	151
Hornblende Andesite	3400	2.474	Ranalli (1997)	3.2×10^{-1}	2.4	293
Granite	5800	2.667	Ranalli (1997)	2×10^{-4}	1.9	137
Limestone	5000	2.600	Fernández and Ranalli (1997)	3.3×10^{-6}	2.4	134
Vescicular Andesite	5500	2.570	A1) Ranalli (1997)	3.3×10^{-4}	3.2	238
			A2) Carcione et al. (2014)	10^2	2	134
Basalt	6400	2.772	A1) Violay et al. (2012)	6.1×10^8	3.6	456
			A2) Carcione et al. (2014)	10^2	2	134

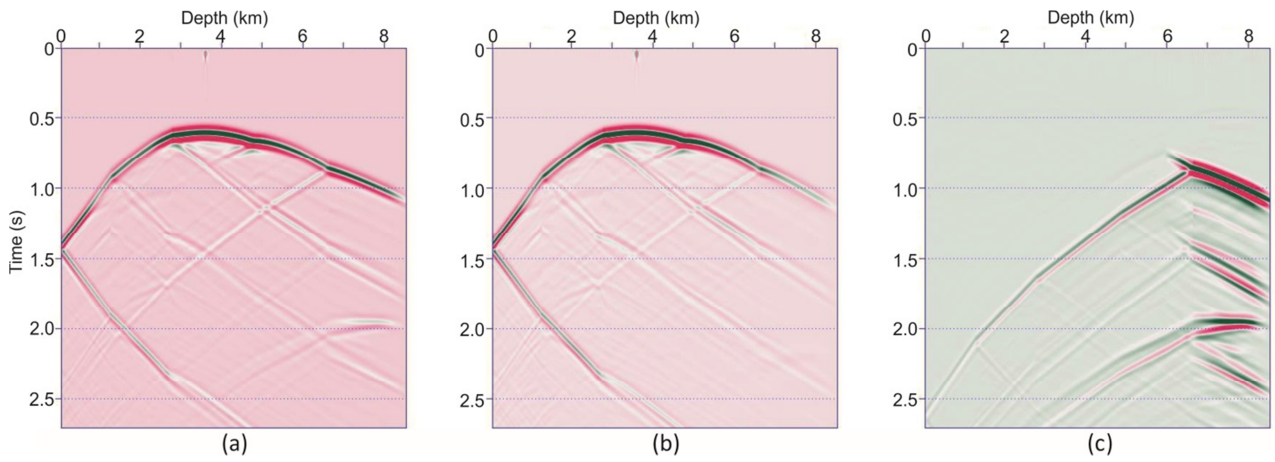


Figure 10: VSP acquired assuming a source at depth. a) In the absence of melting. b) with melting, and c) difference. We observe a clear variation of the synthetic signal in the melting zone. However also the reflection predicting the interface of the melting formation from shallower depths changes its magnitude, as shown by the upgoing events in panel (c).

Figure 10a shows the synthetic VSP, pressure waves, recorded under superhot conditions, but without reaching the limit of melting. Figure 10b is the result obtained with melting at depth, below 6 km, where there is attenuation of the direct P-wave arrivals, and also shear-wave conversion. The variation is clear in (c), obtained as the difference of (a) and (b), also at measurement depths shallower than 6 km for reflections.

4.2 Hot chimney detection

In the second scenario, we use the same geometry and model with and without the presence of the hot chimney (Fig. 11 and Fig. 9, respectively). In the first case, the temperature of the chimney is 400°C , higher than that of the superhot surrounding zone. In the second case (without chimney), its temperature is the same of the unperturbed formation (Figure 9). A simulation with the source at the same position of the previous example and receivers located at opposite sides of the chimney with respect to the source makes it possible to measure direct waves travelled through the chimney.

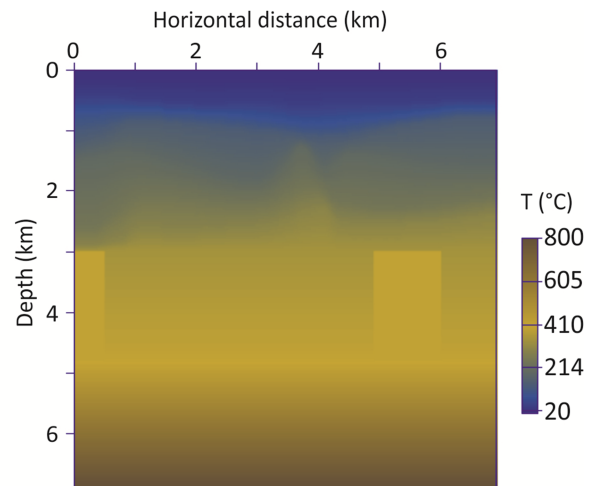


Figure 11: Temperature model with schematized superhot chimneys used for full waveform synthetic simulation and evaluation of effects on seismic wave-field propagation. To simulate the corresponding results in the model without chimneys, we used the model of Figure 9, where the temperatures are shown using different colour scales.

The difference between the two physical corresponds to different observable seismic results

Figure 12 shows the shots recorded with a line of geophones at the surface with and without the chimney. Figure 12a shows the result obtained with the superhot chimney, and Figure 12b shows the results obtained without the superhot chimney, whereas Figure 12c shows the difference. In this case, the variation is observable at the surface.

5. CONCLUSIONS

We have reviewed the physics to simulate seismic-wave properties and compute synthetic wave-fields in geothermal reservoirs as a function of temperature and confining pressure. The approach is based on heterogeneous poro-viscoelastic media.

In the application to hot and superhot systems, we introduce the concept of characteristic melting depth point, based on the melting rate observed in the seismic velocity, showing that this point is different

for P and S waves. The analysis is used for the estimation of melting as a function of depth, and hence with confining pressure, according to literature results in wet rocks. The analysis is then applied for full-waveform simulation in heterogeneous media, specifically in the Los Hornos superhot Mexican caldera and geothermal site.

The simulation provides an analysis tool and makes it possible to detect differences in the seismic wave-fields due to temperature effects, in surface and borehole measurements. Obviously, the repeatability conditions obtainable by synthetic data are not obtainable in nature, and the approach has to be adapted for full-waveform analysis of seismic data, with comparison and calibration of synthetic data and real measurements of deep structures.

Acknowledgements

This project has received funding from the European Union's Horizon 2020 research and innovation programme under grant agreement No. 727550.

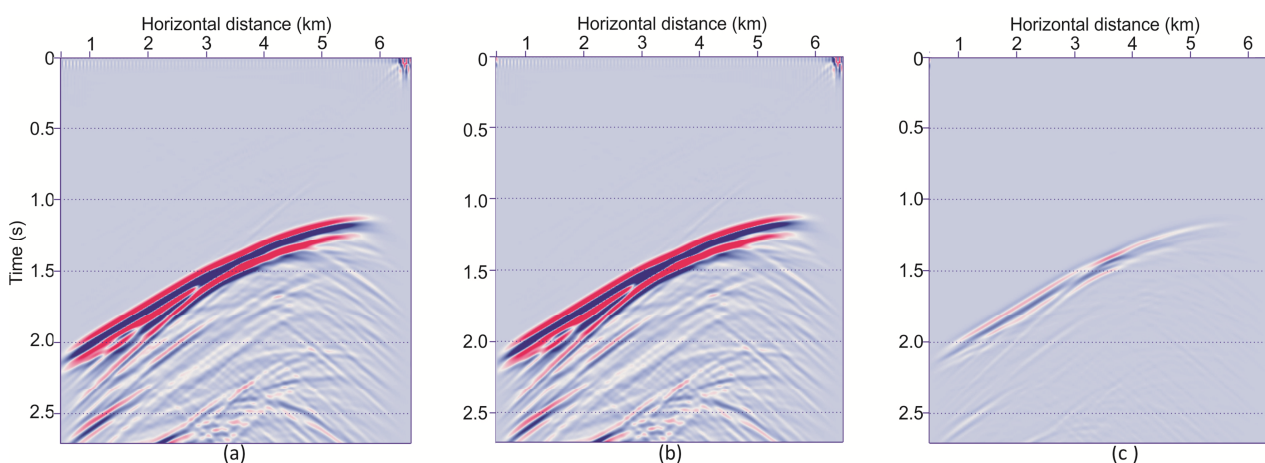


Figure 12: Signal of the surface seismic line acquired a) in the model with superhot chimney, b) in the model without superhot chimney, and c) difference of the results (a) and (b).

REFERENCES

- Carcione, J. M., and Poletto, F., 2013. Seismic rheological model and reflection coefficients of the brittle-ductile transition, *Pure and Applied Geophysics*, DOI 10.1007/s00024-013-0643-4.
- Carcione, J. M., Poletto, F., Farina, B. and Craglietto, A., 2014. Simulation of seismic waves at the Earth crust (brittle-ductile transition) based on the Burgers model, *Solid Earth*, 5, 1001-1010.
- Carcione, J. M., Poletto, F., Farina, B., and Craglietto, A., 2017. The Gassmann-Burgers model to simulate seismic waves at the Earth crust and mantle, *Pure and Applied Geophysics*, 174, 849-863. DOI: 10.1007/s00024-016-1437-2.
- Carrasco-Núñez G., López-Martínez M., Hernández J., and Vargas V., 2017. Subsurface stratigraphy and its correlation with the surficial geology at Los Humeros geothermal field, eastern Trans-Mexican volcanic belt. *Geothermics*, 67, 1-17.
- Farina, B., Poletto, F., Carcione, J., 2016. Seismic wave propagation in poro-viscoelastic hot rocks. In: *Proceedings, European Geothermal Congress 2016*, Strasbourg, France, p 7.
- Farina, B., Poletto, F., Mendrinós, D., Carcione, J. M., and Karytsas, C., 2019. Seismic properties in conductive and convective hot and super-hot geothermal systems. Paper submitted to *Geothermics*.
- Fernández, M., and Ranalli, R., 1997. The role of rheology in extensional basin formation modelling. *Tectonophysics*, 282, 129-145.
- Jaya, M. S., Shapiro, S. A., Kristinsdóttir, L. H., Bruhn, D., Milsch, H., Spangenberg, E., 2010. Temperature dependence of seismic properties in geothermal rocks at reservoir conditions. - *Geothermics*, 39, 1, pp. 115-123. DOI: <http://doi.org/10.1016/j.geothermics.2009.12.002>.
- Lambert, I. B. and Wyllie, P. J., 1972. Melting of gabbro (quartz eclogite) with excess water to 35 kilobar, with geological implications. *Journal of Geology*, v. 80, p 693-708
- Poletto, F., Farina, B., and Carcione, J. M., 2018. Sensitivity of seismic properties to temperature variations in a geothermal reservoir, *Geothermics*, 76, 149—163.
- Poletto and Miranda, 2004. *Seismic While Drilling. Fundamentals of Drill-bit Seismic for Exploration*. Elsevier, Vol. 35.
- Popp, T., and Kern, H., 1994. The influence of dry and water saturated cracks on seismic velocities of crustal rocks - A comparison of experimental data with theoretical model. *Surveys in Geophysics*, 15, 443-465.
- Ranalli, 1997. *Rheology of the lithosphere in space and time*. Geological Society, London, Special Publications 1997, V. 121, 19-37
- Schilling, F. R., Trumbull, R. B., Brasse, H., Haberland, C., Asch, G., Bruhn, D., Mai, K., Haak, V., Giese, P., Muñoz, M., Ramelow, J., Rietbrock, A., Ricaldi, E. and Vietor, T., 2006. Partial Melting in the Central Andean Crust: a Review of Geophysical, Petrophysical, and Petrologic Evidence. In book: *The Andes*. DOI: 10.1007/978-3-540-48684-8_22
- Verma M.P., Surendra, P. Verma, and Sanvincente H., 1990. Temperature field simulation with stratification model of magma chamber under Los Humeros caldera, Puebla, Mexico. *Geothermics*, 19 (2), 187-197.
- Violay, M., Gibert B., Mainprice D., Evans B., Dautria J. M., Azais P., and Pezard, P., 2012. An experimental study of the brittle-ductile transition of basalt at oceanic crust pressure and temperature conditions. *Journal of Geophysical Research*, 117.